

Title: Fusion of RVG or gh625 to Iduronate-2-Sulfatase for the Treatment of Mucopolysaccharidosis Type II

Authors: Shaun R. Wood¹, Ahsan Chaudrhy¹, Stuart Ellison¹, Rachel Searle¹, Constance Burgod¹, Ghazala Tehseen¹, Gabriella Forte¹, Claire O'Leary¹, H el ene Gleitz², Aiyin Liao³, James Cook¹, Rebecca Holley¹ and Brian W. Bigger¹

¹ Division of Cell Matrix Biology and Regenerative Medicine, University of Manchester, Manchester, UK

² Division of Cell Matrix Biology and Regenerative Medicine, Erasmus University, Rotterdam, the Netherlands

³ University College London, London, UK

Corresponding author:

Brian.Bigger@manchester.ac.uk

Abstract:

Mucopolysaccharidosis type II (MPSII) is a lysosomal storage disease caused by a mutation in the *IDS* gene, resulting in deficiency of the enzyme iduronate-2-sulfatase (IDS) causing heparan sulfate (HS) and dermatan sulfate (DS) accumulation in all cells. This leads to skeletal and cardiorespiratory disease with severe neurodegeneration in two thirds of sufferers. Enzyme replacement therapy is ineffective at treating neurological disease, as intravenously-delivered IDS is unable to cross the blood-brain barrier (BBB). Haematopoietic stem cell transplant is also unsuccessful, presumably due to insufficient IDS enzyme production from transplanted cells engrafting in the brain. We used two different peptide sequences (RVG and gh625), both previously published as BBB-crossing peptides, fused to IDS and delivered via haematopoietic stem cell gene therapy (HSCGT). HSCGT with LV.IDS.RVG and LV.IDS.gh625 was compared to LV.IDS.ApoEII and LV.IDS in MPSII mice at 6-months post-transplant. Levels of IDS enzyme activity in the brain and peripheral tissues were lower in LV.IDS.RVG and LV.IDS.gh625 treated mice than in LV.IDS.ApoEII and LV.IDS treated mice, despite comparable vector copy numbers. Microgliosis, astrocytosis and lysosomal swelling were partially normalised in MPSII mice treated with LV.IDS.RVG and LV.IDS.gh625. Skeletal thickening was normalised by both treatments to wild-type levels. Although reductions in skeletal abnormalities and neuropathology are encouraging, given the low levels of enzyme activity compared to control tissue from LV.IDS and LV.IDS.ApoEII transplanted mice, the RVG and gh625 peptides are unlikely to be ideal candidates for HSCGT in MPSII, and are inferior to the ApoEII peptide that we have previously demonstrated to be more effective at correcting MPSII disease than IDS alone.

Introduction:

Mucopolysaccharidosis type II (MPSII) is a lysosomal storage disorder caused by mutations in the *Iduronate-2-Sulfatase (IDS)* gene. This leads to a deficiency of the IDS enzyme, causing a build-up of the glycosaminoglycans (GAGs) heparan sulfate (HS) and dermatan sulfate (DS) in the lysosomes. MPSII is characterised by skeletal abnormalities, cardio-respiratory complications and, in around two-thirds of patients, neurological decline [1]. Current treatment options for MPSII, such as enzyme replacement therapy, are able to alleviate non-neurological pathology yet have little effect on neurological outcomes due to the blood-brain-barrier (BBB) preventing large molecules from entering the CNS. Unlike in the related condition MPSI, haematopoietic stem cell transplant (HSCT) is largely ineffective at treating the CNS, probably due to the levels of enzyme secreted from engrafted cells being insufficient to treat the disease [2].

We have demonstrated that a haematopoietic stem cell gene therapy (HSCGT) approach, utilising a lentiviral vector expressing codon-optimised *IDS* was able to reduce HS storage and improve behavioural outcomes in the mouse model of MPSII. Furthermore, the addition of a BBB-targeting peptide sequence, a tandem repeat of the receptor binding domain of ApoE (ApoEII), further improved neurological correction over the native enzyme alone [3]. Typically, HSGCT results in high enzyme levels (2-20 fold of normal) in the periphery, but only a fraction of normal enzyme levels in the brain [4]. As such, the use of BBB-targeting peptides may facilitate the crossing of this peripheral enzyme into the brain.

In this study, we analysed two other peptide sequences for their ability to improve uptake of IDS enzyme into the brain. 'RVG' is based on the rabies virus glycoprotein, which binds to the N-acetylcholine receptor, while 'gh625' is derived from the herpes simplex virus. Both these viral derived peptide sequences have been shown to facilitate transport of molecules across the BBB in several studies [5-7]. We fused these peptides to IDS via a flexible linker and packaged them into third-generation lentiviral vectors. These vectors were used to transduce lineage-depleted murine bone marrow cells that were transplanted into conditioned MPSII mice. Mice were analysed at 6 months post-

transplant for behavioural and biochemical outcomes. The data was compared to LV.IDS and LV.IDS.ApoEII samples from a previous experiment as controls.

Methods:

Expression vectors

The brain-targeting peptide sequences RVG (YTIWMPENPRPGTTPCDIFTNSRGKRASNG) and gh625 (HGLASTLTRWAHYNALIRAF) were inserted downstream of the human *IDS* cDNA in the third-generation LV (pCCL.sin.cPPT.hCD11b.IDS.WPRE (LV.IDS)), using the long invariant linker (LGGGGSGGGGSGGGGSGGGGS) and were subsequently cloned into the same third-generation lentiviral backbone to create LV.IDS.RVG and LV.IDS.gh625.

LV production and titration

Lentiviral vectors were produced by transfection of HEK293T cells with pRSV-Rev, pMDLg/pRRE, pMD2.G and LV expression plasmid and 7.5mM polyethylenimine (40kDa, Polysciences) [8]. Lentiviral titration was performed as previously described [9].

Uptake and Transcytosis Assays

Human CHME3 cells were transfected with 2 µg of CD11b.IDS or CD11b.IDS.RVG or CD11b.IDS.gh625 plasmid DNA using 7.5 mM high potency linear polyethylenimine (PEI - pH 7.4, 40 kDa; Polysciences Inc., Warrington, PA, USA) and 150 mM NaCl. Media was collected after 48 hours. Human IDS protein was detected using the Human Iduronate-2-Sulfatase DuoSet ELISA kit according to the manufacturer's instructions (R&D Systems, Abingdon, UK). For uptake studies, ~20 ng of IDS, IDS.RVG or IDS.gh625 was added to bEND.3 cells following seeding at 10,000 cells/cm² for 3 days for monolayer culture. For transcytosis studies, ~70 ng of IDS, IDS.RVG or IDS.gh625 was added to bEND.3 cells following seeding at 50,000 cells/cm² for 5 days on the luminal side of Thincerts (0.4 µm pore size, translucent PET). For uptake assays, cell lysate was collected after 3 hours and for transcytosis assays, media was collected after 3 hours. IDS expression in cell lysate/media was detected using the Human Iduronate-2-Sulfatase DuoSet ELISA kit according to the manufacturer's instructions.

Mice and transplant procedures

Female heterozygous for the X-linked allele on a C57BL/6 background were obtained from Prof. Joseph Muenzer (University of North Carolina at Chapel Hill, NC, USA) and bred with wild-type (WT) C57BL/6J males (Envigo, Alconbury, UK) to obtain affected males, carrier females and WT animals (male and females). MPSII mice were backcrossed onto a Pep3 CD45.1 congenic background (B6.SJL-PtprcaPepcb/BoyJ) to distinguish donor and recipient cells following transplant. Wild-type littermates were used as controls throughout. Group sizes were n=4-7, determined by power calculations. This study was approved by the Ethics Committee of the University of Manchester. They were conducted under licence from the Home Office in accordance with British legislation and the European Communities Council Directive 86/609/EEC for the care and use of experimental animals.

For transplantation studies, total bone marrow mononuclear cells from MPSII/Pep3 mice (CD45.1) were isolated and lineage depleted using the murine lineage cell depletion kit (Miltenyi Biotec, Bisley, UK) in accordance with the manufacturer's instructions. Cells were stimulated using 100 ng/ml murine stem cell factor, 100 ng/ml murine fms-like tyrosine kinase-3 and 10 ng/ml recombinant murine interleukin-3 (PeproTech, Rocky Hill, NJ, USA) for 3 hours prior to transduction with a lentiviral vector (expressing either IDS, IDS.ApoEII, IDS.RVG or IDS.gh625) at a MOI of 100.

Six-to-eight-week-old mice were myeloablated using 125 mg/kg Busulfan (Busilvex; Pierre Fabre, Boulogne, France) in five daily doses (25mg/kg/day) via i.p. injection. Within 24 hours of myeloablation, mice received $3-4 \times 10^5$ lineage-depleted transduced haematopoietic stem cells through the lateral tail vein.

Chimerism analysis using flow cytometry

Engraftment of donor cells was assessed at ~4 weeks post-transplant in peripheral blood, by staining leukocytes with anti-mouse CD45.1-PE (donor leukocytes), anti-mouse CD45.2-FITC (recipient leukocytes) (both Fisher Scientific Ltd.) in 5 μ M ToPro3 Iodide (ThermoFisher). Analysis was performed on a BD FACS Canto II flow cytometer (BD Biosciences).

X-ray imaging of live mice

Control and treated mice were anesthetized using isoflurane (induction: 3L/min in pure O₂, maintenance: 1.5L/min in pure O₂) and radiographed (45keV) using the Bruker InVivo Xtreme system. X-ray images were analysed using ImageJ.

Sample processing

At 8 months of age, mice were anesthetized and perfused with room temperature PBS. One brain hemisphere was fixed in 4% paraformaldehyde (PFA) for 24 hours, transferred to 30% sucrose, 2 mmol/l MgCl₂/phosphate-buffered saline solution for 48 hours before freezing at -80°C. Samples of brain, spleen and liver were snap-frozen on dry ice. For enzyme activity assays, samples were homogenized and sonicated in homogenization buffer (0.5M NaCl, 0.02M Tris, 0.1% Triton-X100, pH 7). Genomic DNA used for organ VCN analysis was extracted using GenElute Mammalian Genomic DNA Miniprep kit (Sigma).

Enzyme activity assays

IDS enzyme activity was measured in a two-step protocol using the fluorescent substrate MU- α IdoA-2S (Carbosynth) and Aldurazyme (Genzyme) as previously described [10]. Starting material was standardized to 20 μ g of total protein for plasma, 40 μ g for liver and spleen and 60 μ g for brain using a BCA assay (ThermoFisher). Fluorescence was measured using the Biotek Synergy HT plate reader (excitation: 360 nm, emission: 460 nm).

Immunohistochemistry (IHC)

Free-floating IHC was performed on 30 μ m PFA-fixed coronal brain sections using rabbit anti-NeuN (1:1000, ab177487, Abcam PLC, Cambridge, UK), rabbit anti-GFAP (1:1500, Z0334, Dako, Stockport, UK) and rat anti-LAMP2 (1:500, ab13524, Abcam) primary antibodies using standard protocols. Isolectin B4 (ILB4, 5 μ g/ml, L5391, Sigma) was visualized on 30 μ m coronal brain sections using DAB substrate for 40 seconds (Vector, Peterborough, UK) using standard protocols. Images were acquired on a 3D-Histech Panoramic-250 microscope slide-scanner using a 20x/ 0.30 Plan Achromat objective (Zeiss) with extended focus and the DAPI, FITC and TRITC filter sets. Snapshots of the slide-scans were taken using Case Viewer software (3D-Histech). Nonlinear adjustments were

made to all immunofluorescence images equally to eliminate background; gamma 0.72, input levels 0-190. GFAP immunofluorescence was quantified using ImageJ software on 4 sections per mouse for cortex, and 1 section per mouse for the amygdala (n=3/group). Counts of ILB4-positive cells were performed on 4 sections per mouse at 20x magnification and counted manually using ImageJ software.

Vector Copy Number (VCN)

VCN was determined from harvested tissue using quantitative PCR as previously described [9].

Statistics

Statistical analysis was performed using GraphPad Prism 7 software (La Jolla, CA, USA). Following normality testing, two-tailed parametric unpaired t-tests were applied for individual group comparisons. Either one-way ANOVAs followed by Tukey's multi-comparisons test (parametric) or Kruskal-Wallis test (non-parametric) were performed for multi-group analysis. Significance was set at $p < 0.05$.

Results:

Outcomes at 6-months post-transplant in LV.IDS.RVG and LV.IDS.gh625 treated mice were compared to control tissue from previously transplanted LV.IDS and LV.IDS.ApoEII transplanted mice [3].

Addition of gh625, but not RVG, increases uptake into bEND.3 cells *in vitro*.

To analyse changes in uptake and transcytosis *in vitro*, bEND.3 cells were used as a model of the blood-brain-barrier. Increases in intracellular IDS expression were seen in bEND.3 cells when cultured with IDS.gh265 compared to IDS and IDS.RVG (figure 1A). No increases, compared to IDS, were seen in transcytosis across bEND.3 monolayers when IDS.RVG and IDS.gh625 were applied (figure 1B).

Transduction of lineage-depleted murine bone marrow gives detectable levels of IDS.RVG and IDS.gh625 in cells pre-transplant.

Following transduction of lineage-depleted bone marrow, an IDS enzyme activity assay and qPCR were used to assess the detectable IDS activity and VCN, respectively, in cells prior to transplant. Both groups produced detectable levels of IDS activity, with greater activity seen in the IDS.RVG transduced cells (figure 2A) with the IDS.RVG group also demonstrating the highest VCN (figure 2B). Chimerism was analysed using flow cytometry, one month post-transplant (figure 2C). Chimerism in IDS.gh625-treated animals (87.73%) was higher than IDS.RVG treated animals (82.03%) but this was not significant when analysed with an un-paired t-test ($p=0.0774$).

HSCGT with IDS.RVG and IDS.gh625 in MPSII mice generates detectable IDS activity throughout the body.

Samples of brain, liver and spleen were analysed for IDS enzyme activity and detectable VCN 6 months post-transplant. Levels of IDS activity in IDS.RVG and IDS.gh625-treated animals was about 4.08% and 1.84% of WT expression in the brain, respectively (compared to 19.54% and 21.38% for IDS and IDS.ApoEII, respectively, figure 2D). In the liver, expression was 173% and 68% of WT for IDS.RVG and IDS.gh625, respectively (compared to 2073% and 2379% for IDS and IDS.ApoEII, respectively, figure 2E). In the spleen, expression was 526% and 108% of WT for IDS.RVG and IDS.gh625, respectively (compared to 4925% and 2634% for IDS and IDS.ApoEII, respectively, figure 2F). Vector copies were detected in all organs, with IDS.RVG-treated animals demonstrating higher VCN in all organs (figure 2G-I). When normalised to VCN, IDS activity in the brain was greatest in IDS.gh625 treated animals (however this was not statistically significant via one-way ANOVA compared to IDS – figure 2J). In the liver, normalised IDS activity was significantly lower in both IDS.RVG and IDS.gh625 treated animals compared to IDS treated. IDS.ApoEII treated animals had significantly greater normalised IDS activity than IDS, IDS.RVG or IDS.gh625-treated animals via one-way ANOVA (figure 2K). Normalised IDS activity in the spleen was significantly lower in IDS.RVG and IDS.gh625 treated animals compared to both IDS and IDS.ApoEII treated animals via one-way ANOVA (figure 2L).

LV.IDS.RVG and LV.IDS.gh625 mediate limited reduction in lysosomal accumulation in neurons throughout the brain.

To determine the effects of increased IDS enzyme activity in the brains of transplanted MPS II mice 6 months post-transplantation, the lysosomal marker LAMP2 was used to stain coronal brain sections of control and treated MPS II mice for lysosomal compartment size. The neuronal marker 'NeuN' used for substrate accumulation in neurons. WT animals displayed weak, punctate and perinuclear LAMP2 staining that only partially co-localised with NeuN in the motor cortex. Untreated MPS II mice displayed strong co-localised staining of NeuN and LAMP2 in multiple areas of the brain; including the motor cortex, caudate putamen, hippocampus and amygdala, suggesting a substantial lysosomal burden in neurons (figure 3A). In MPS II mice, LAMP2 quantification was increased 3.5-fold and 4.9-fold compared to WT. Treatment groups LV.IDS.RVG and LV.IDS.gH625 both mediated significant reductions in LAMP2 staining in the amygdala (2.6-fold and 3.3-fold of WT levels) and a trend to reduction in the motor cortex (1.9-fold and 2.3-fold of WT levels) and the (figure 3B-C).

LV.IDS.RVG and LV.IDS.gH625 mediate improvement in neuro-inflammation in MPS II mice.

In MPS disorders, neuro-inflammatory responses are driven by astrocytes, which can result in reactive gliosis, astrogliosis and increased levels of inflammatory cytokines. GFAP (green), an astrocytic marker, and LAMP2 (red), a lysosomal marker, were used to stain coronal brain sections of control and treated MPS II mice. WT mice displayed minimal GFAP staining. However, in untreated MPS II mice there was considerable staining of GFAP in the cortex, caudate putamen, hippocampus and amygdala indicating astrogliosis (figure 4A). In untreated mice, strong co-localisation of GFAP and LAMP2 was observed in the cortex, caudate putamen, hippocampus and amygdala, which is indicative of lysosomal substrate accumulation in astrocytes, as well as neurons. GFAP quantification in untreated MPS II mice was 7-fold higher in the cortex and 8.1-fold higher in the amygdala relative to WT levels. LV.IDS.RVG and LV.IDS.gH625 both demonstrate a significant reduction in the levels of reactive

astrocytes that are present in the cortex (2.9-fold and 3.4-fold of WT levels) and amygdala (3.6-fold and 4.8-fold of WT levels) (figure 4B-C).

LV.IDS.RVG significantly reduces numbers of ILB4-positive cells thereby improving neuro-inflammation.

In the brains of untreated MPS II mice, there is a significant increase in the number of ILB4-positive cells. A 23-fold and 34-fold increase in activated microglia is seen in the cortex and striatum, respectively. Therefore this increase signifies substantial microgliosis and subsequent neuro-inflammation in these animals. WT mice have minimal numbers of activated microglial cells in the cortex and striatum (figure 5A). Treated mice reduced ILB4 staining and activated microglia to 9-fold and 12-fold of WT levels in the cortex and 14-fold and 19-fold of WT levels in the striatum for LV.IDS.RVG and LV.IDS.gH625 respectively (Figure 5B-C). This was a significant reduction for LV.IDS.RVG but not for LV.IDS.gH625. Levels of ILB4-positive cells were substantially reduced in treated mice compared to untreated MPS II animals.

Skeletal rescue is observed with LV.IDS.RVG and LV.IDS.gH625 in MPS II mice

In order to collect data on the extent of skeletal symptoms, total body X-ray radiography was performed under anaesthesia on control and treated mice. In MPS II mice, the widths of the zygomatic arches, humeri and femurs are all increased over WT mice. Both LV.IDS.RVG and LV.IDS.gH625 were able to reduce zygomatic arch width to WT levels (figure 6A and 6D). Humerus widths for the treated groups were also reduced to near WT dimensions, but not completely normalised (figure 6B and 6E). Moreover, the femur widths in the LV.IDS.RVG treated animals were significantly thinner than MPS II mice (figure 6C and 6F). LV.IDS.gH625 femur widths were not significantly reduced from MPSII.

Discussion:

HSCGT has shown promise in pre-clinical studies for MPSII as well as MPSI, MPSIIIA and MPSIIIB [3, 8, 11, 12]. In MPSII, both we and others have seen that the use of HSCGT with LV.IDS can alleviate the disease phenotype in MPSII mice, however it does not achieve full

correction [3, 13]. In our previous study, we used IDS tagged to a BBB-crossing peptide (ApoEII) designed to improve uptake of enzyme into cells following transplant. LV.IDS.ApoEII demonstrated superior correction of behaviour, GAG storage and inflammatory markers compared to LV.IDS [3].

In this study we sought to compare two other peptide constructs for their ability to improve uptake of IDS across the BBB to treat MPSII following HSCGT. RVG and gh625 are peptides based on the rabies virus glycoprotein and herpes simplex virus respectively and both have demonstrated potential for increasing BBB uptake [5-7].

HSCGT treatment with both constructs reduced lysosomal swelling in the brain cortex and amygdala, as demonstrated by LAMP2 staining (figure 3), however only reductions in the amygdala were statistically significant. Reductions were also seen in astrocytosis, as demonstrated by GFAP staining, with IDS.RVG demonstrating a significant increase in reduction over IDS.gh625 in the amygdala (figure 4). Both IDS.RVG and IDS.gh625 facilitated reductions in microgliosis, as demonstrated by ILB4 staining (figure 5), however only IDS.RVG produced a statistically significant result.

We are able to compare these data against those of Gleitz et al, 2018 as the experiments were performed identically. In comparison to the data presented in Gleitz et al, 2018, the correction seen in the brain is far less impressive with IDS.RVG or IDS.gh625 than with IDS.ApoEII. We saw partial correction with both IDS.RVG and IDS.gh625 compared to full correction with IDS.ApoEII of LAMP2 staining in the cortex and amygdala, astrocytosis in the cortex and amygdala and microgliosis in the cortex and striatum [3]. Therefore, the increased activity per VCN seen in the IDS.gh625 group is not translating to a better neuropathological outcome. IDS.RVG and IDS.gh625 also significantly reduced skeletal thickening in the zygomatic arches and humerus (figure 6 D-E). Only IDS.RVG significantly reduced femur thickness (figure 6F). Skeletal outcomes in this study were similar as they were with IDS.ApoEII [3].

Biochemical analyses of IDS.RVG and IDS.gh625-treated animals were compared to samples reanalysed from our previous study (IDS and IDS.ApoEII-treated animals) as control samples. Analysis of IDS activity in the brain showed that transplanted cells

12

transduced with IDS.gh625 produced less activity than those transduced with IDS.RVG (figure 2D). However, looking at the VCN analysis in the cells prior to transplant (figure 2B) and the VCN in figure 2G, this is likely to be down to a lower level of transduction at the start of the experiment. What's interesting is that, despite this lower level of activity, correction is still good in the brain. When normalised to VCN it also seems that more IDS.gh625 is present in the brain than IDS, IDS.ApoEII or IDS.RVG (figure 2J). This could potentially be due to an increase in uptake into the brain, which is consistent with uptake data seen *in vitro* in bEND.3 cells (figure 1A), however if this were the case, an improvement in neurological outcomes might be expected. It is also worth noting that the VCN analysis in the brain is more challenging than in other organs, due to the relatively small number of cells that engraft in the brain following transplant [4]. A final explanation for this could be that the RVG and ApoEII tags (both of which produced less activity in the brain than native IDS when normalised to VCN) are interfering with the enzyme activity. Whilst this may be the case for RVG, it's unlikely to be the case for ApoEII as we would expect to see reduced activity in the liver and spleen compared to native IDS and, in both tissues, IDS.ApoEII activity is equal or better than IDS. We feel that the data shown here indicates that the interaction between the tag and the enzyme is more important than the tag alone. Both gh625 and RVG have demonstrated the ability to increase transport across the BBB into the brain [5-7] however, when tagged to IDS, they appear to be ineffective. It's possible that, in order to improve BBB crossing for lysosomal enzymes, appropriate tags will need to be tailored to the enzyme in question.

Overall, the neurological correction seen in these animals is limited and does not appear to be as great as in IDS.ApoEII-treated animals as previously demonstrated. For IDS.gh625, this is in spite of a much greater IDS activity/VCN in the brain compared to previously published results [3]. Therefore despite the fact that both peptides were able to mediate somatic correction of skeletal phenotypes and partial correction of brain pathology such as lysosomal storage (LAMP2), and inflammation (GFAP and ILB4), RVG and gh625 are unlikely to be good candidates to improve HSCGT for MPSII patients compared to IDS.ApoEII. In conclusion, the nature of the RVG and gh625 peptides, based on viral glycoproteins, could have contributed to the fact that although they provided encouraging

data in some assays, in vitro and in vivo, neither one was as effective as the ApoEII peptide at ameliorating disease symptoms and correcting behaviour in MPSII mice. It is likely that improving uptake of enzymes in the context of HSCGT can add significant benefit to the overall disease correction in the absence of improvements in blood brain barrier crossing.

Acknowledgements

We would like to thank the National MPS Society and the Isaac Foundation for supporting this work. We would also like to thank the Bioimaging Facility at the University of Manchester for their help with obtaining microscope images.

Authorship Contributions

SRW performed experiments, analysed data and wrote the manuscript, AC, RS, CB and GT performed experiments and analysed data. SE performed experiments, analysed data and edited the manuscript. GF, CO'L and JC performed experiments. HFG, AL and RH performed experiments and edited the manuscript. BB obtained the funds, designed the study, analysed the data, and edited the manuscript.

Conflict of Interest

SRW, SE, HG, AL, RH and BWB are beneficiaries of a licenced programme for HSCGT for MPSII from AvroBio. BWB also has unrestricted grants funded by AvroBio.

Funding

National MPS Society; The Isaac Foundation

References:

1. Wraith, J.E., Lysosomal disorders. *Semin Neonatol*, 2002. 7(1): p. 75-83.
2. Wood, S.R. and B.W. Bigger, Delivering gene therapy for mucopolysaccharide diseases. *Front Mol Biosci*, 2022. 9: p. 965089.
3. Gleitz, H.F., Liao, AY, Cook JR, et al., Brain-targeted stem cell gene therapy corrects mucopolysaccharidosis type II via multiple mechanisms. *EMBO Mol Med*, 2018. 10(7).
4. Wilkinson FL, Sergijenko A, Langford-Smith KJ, et al., Busulfan conditioning enhances engraftment of hematopoietic donor-derived cells in the brain compared with irradiation. *Mol Ther*, 2013. 21(4): p. 868-876.
5. Kumar, P., Wu, H, McBride, JL, et al., Transvascular delivery of small interfering RNA to the central nervous system. *Nature*, 2007. 448(7149): p. 39-43.
6. Zadrán S, Akopian G, Zadrán H, et al., RVG-mediated calpain2 gene silencing in the brain impairs learning and memory. *Neuromolecular Med*, 2013. 15(1): p. 74-81.
7. Valiante S, Falanga A, Cigliano L, et al., Peptide gH625 enters into neuron and astrocyte cell lines and crosses the blood-brain barrier in rats. *Int J Nanomedicine*, 2015. 10: p. 1885-1898.
8. Sergijenko A, Langford-Smith A, Liao AY, et al. Myeloid/Microglial driven autologous hematopoietic stem cell gene therapy corrects a neuronopathic lysosomal disease. *Mol Ther*, 2013. 21(10): p. 1938-1949.
9. Langford-Smith A, Wilkinson FL, Langford-Smith KJ, et al., Hematopoietic stem cell and gene therapy corrects primary neuropathology and behavior in mucopolysaccharidosis IIIA mice. *Mol Ther*, 2012. 20(8): p. 1610-1621.
10. Voznyi, Y.V., J.L. Keulemans, and O.P. van Diggelen, A fluorimetric enzyme assay for the diagnosis of MPS II (Hunter disease). *J Inher Metab Dis*, 2001. 24(6): p. 675-680.
11. Holley RJ, Ellison SM, Fil D, et al., Macrophage enzyme and reduced inflammation drive brain correction of mucopolysaccharidosis IIIB by stem cell gene therapy. *Brain*, 2018. 141(1): p. 99-116.

12. Visigalli I, Delai S, Politi LS, et al., Gene therapy augments the efficacy of hematopoietic cell transplantation and fully corrects mucopolysaccharidosis type I phenotype in the mouse model. *Blood*, 2010. 116(24): p. 5130-5139.
13. Wakabayashi T, Shimada Y, Akiyama K, et al. Hematopoietic Stem Cell Gene Therapy Corrects Neuropathic Phenotype in Murine Model of Mucopolysaccharidosis Type II. *Hum Gene Ther*, 2015. 26(6): p. 357-366.

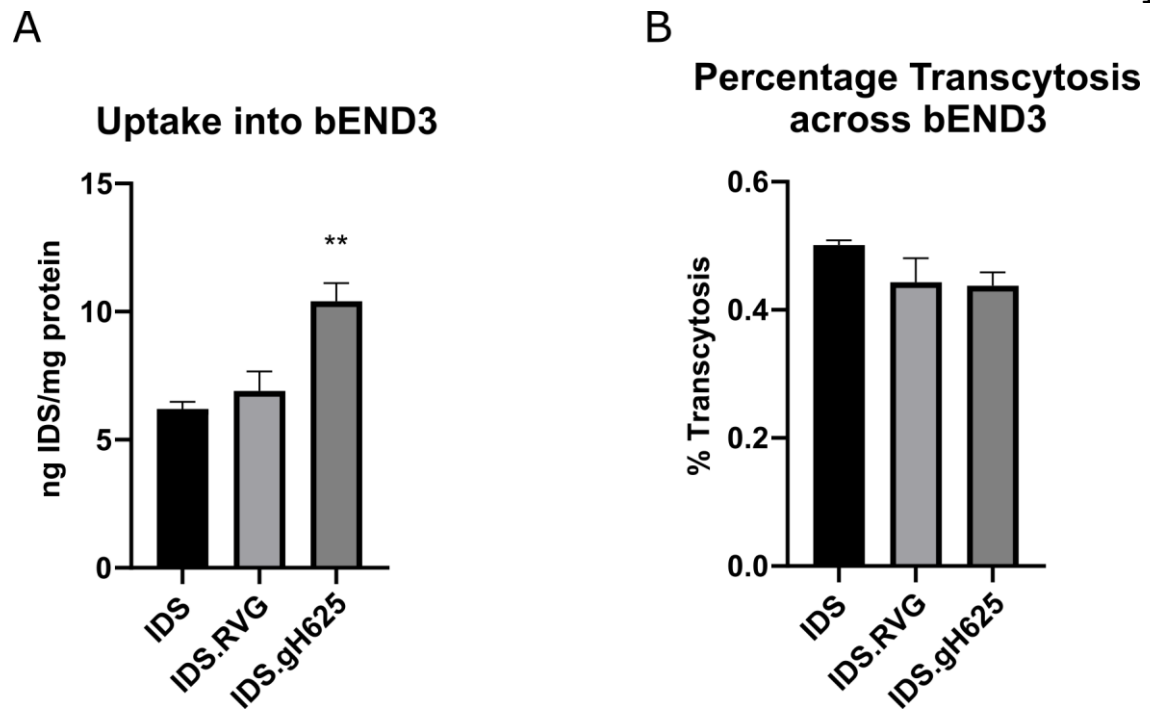


Figure 1. Uptake and Transcytosis in bEND.3 cells *in vitro*. (A) Uptake into bEND3 cells. (B) Transcytosis across bEND.3 monolayers on transwell inserts. Data is displayed as mean ± SEM, ** = $p < 0.01$, compared to IDS via one-way ANOVA.

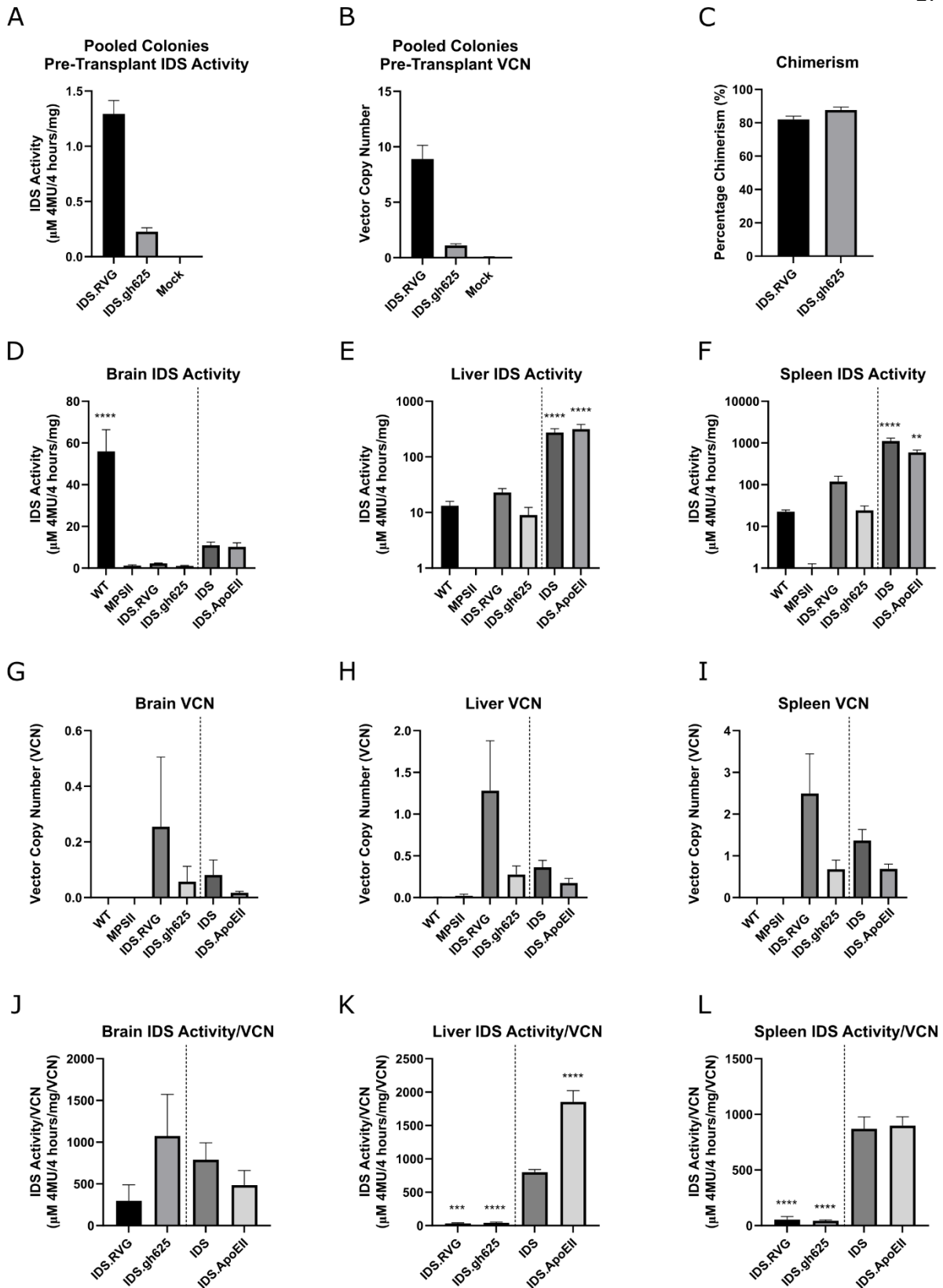


Figure 2. Chimerism, IDS Activity and Vector Copy Number in Treated Animals. (A) IDS activity in colonies pre-transplant. **(B)** VCN in colonies pre-transplant. **(C)** Chimerism in

LV.IDS.RVG and LV.IDS.gh625 treated animals. **(D-F)** Brain, Liver and Spleen 8-months post-treatment. **(G-I)** VCN in Brain, Liver and Spleen 8-months post-treatment. **(J-L)** IDS activity normalised to VCN in Brain, Liver and Spleen. Data is displayed as mean \pm SEM, ** = $p < 0.01$, **** = $p < 0.0001$ compared to MPSII (IDS activity) or IDS (IDS activity/VCN) via one-way ANOVA.

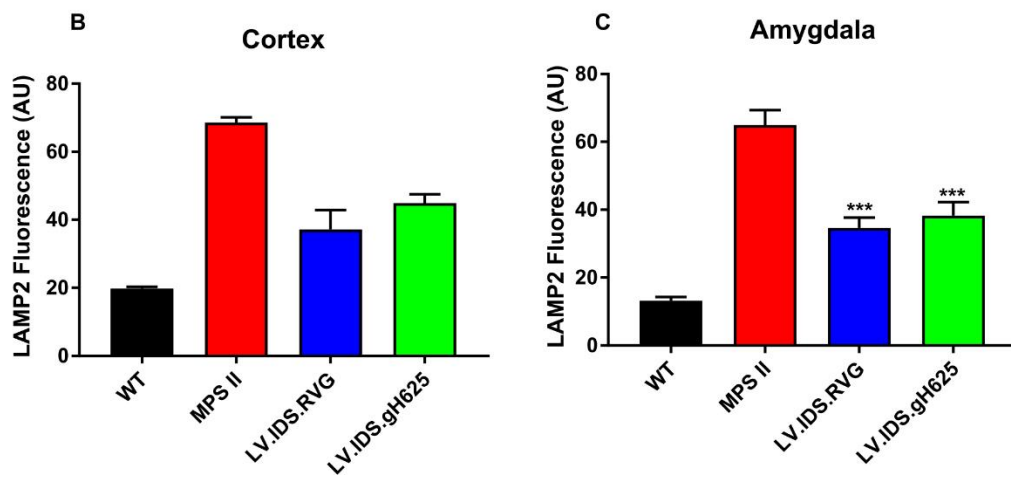
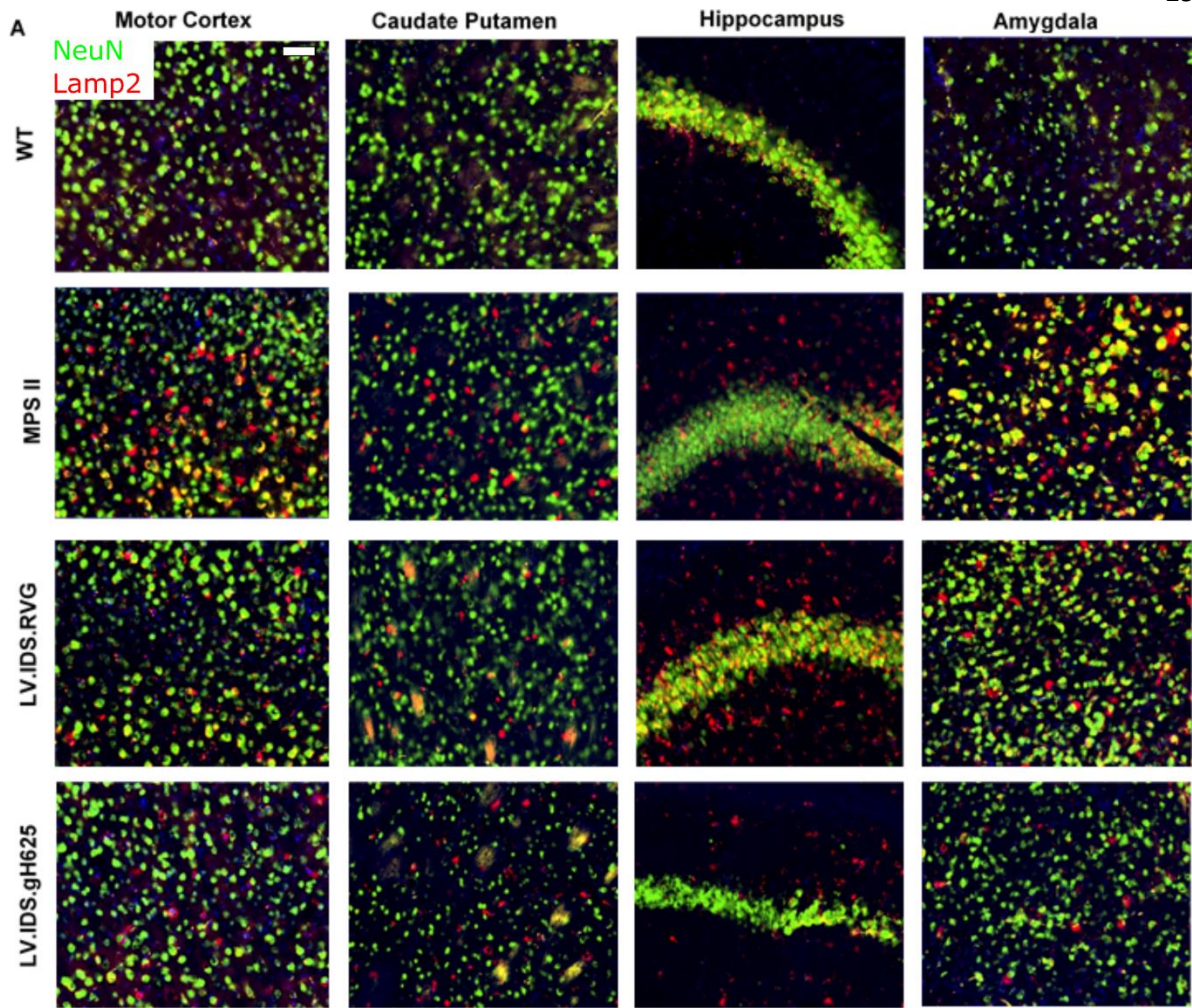


Figure 3. HSCGT with LV.IDS.RVG and LV.IDS.gH625 both reduce neuronal LAMP2 in the amygdala. (A) Representative images of 30µm brain sections of the motor cortex (M2), caudate putamen (both approximately -0.46mm from bregma), hippocampus (CA3) and amygdala (both approximately -1.22mm from bregma) stained with

LAMP2 (lysosomal compartment; red), NeuN (neuronal nuclei; green) and DAPI (nucleus; blue) from control and treated mice. Representative images are shown following staining of 4-7 mice per group, 20x, nonlinear adjustments were made equally in all images to reduce background; gamma 0.80, input levels 0-190. Scale bar = 50 μ m. LAMP2 immunofluorescence was quantified using imageJ in the **(B)** cortex and **(C)** amygdala of MPS II mice 6 months post-transplant. Data is displayed as mean \pm SEM, *** = $p < 0.001$ compared to MPSII via one-way ANOVA.

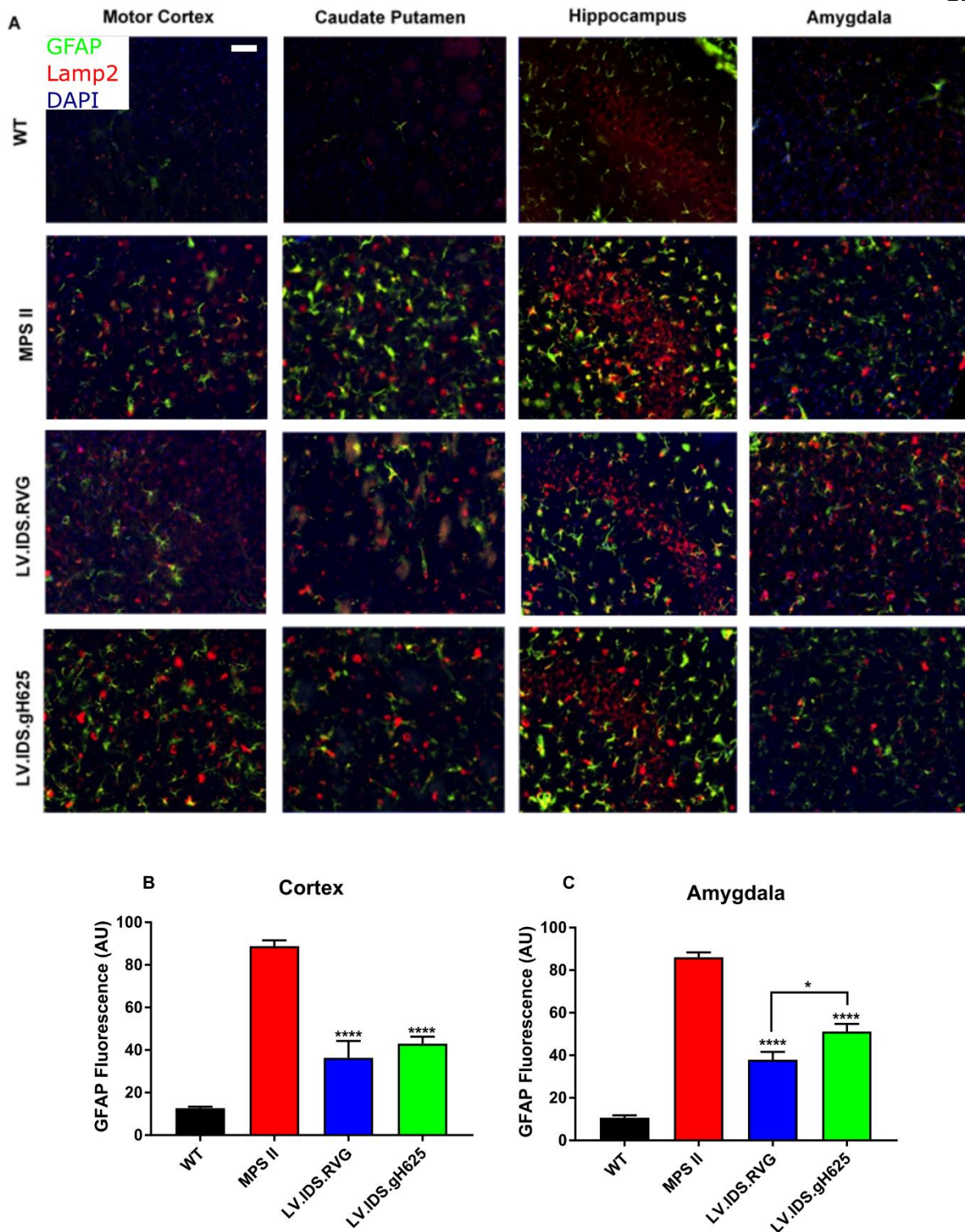


Figure 4. LV.IDS.RVG and LV.IDS.gH625 both significantly correct astrocytic lysosomal swelling and astrocytosis following HSCGT. (A) Representative images of 30µm brain sections of the motor cortex (M2), caudate putamen (both approximately -0.46mm from bregma), hippocampus (CA3) and amygdala (both

approximately -1.22mm from bregma) stained with GFAP (glial fibrillary acidic protein; green), LAMP2 (lysosomal compartment; red) and DAPI (nucleus; blue) from control and treated mice. Representative images are shown following staining of 4-7 mice per group, 20x, nonlinear adjustments were made equally in all images to reduce background; gamma 0.80, input levels 0-190. Scale bar = 50 μ m. GFAP immunofluorescence was quantified using imageJ in the **(B)** cortex and **(C)** amygdala of MPS II mice 6 months post-transplant. Data is displayed as mean \pm SEM, * = $p < 0.05$, **** = $p < 0.0001$ compared to MPSII via one-way ANOVA.

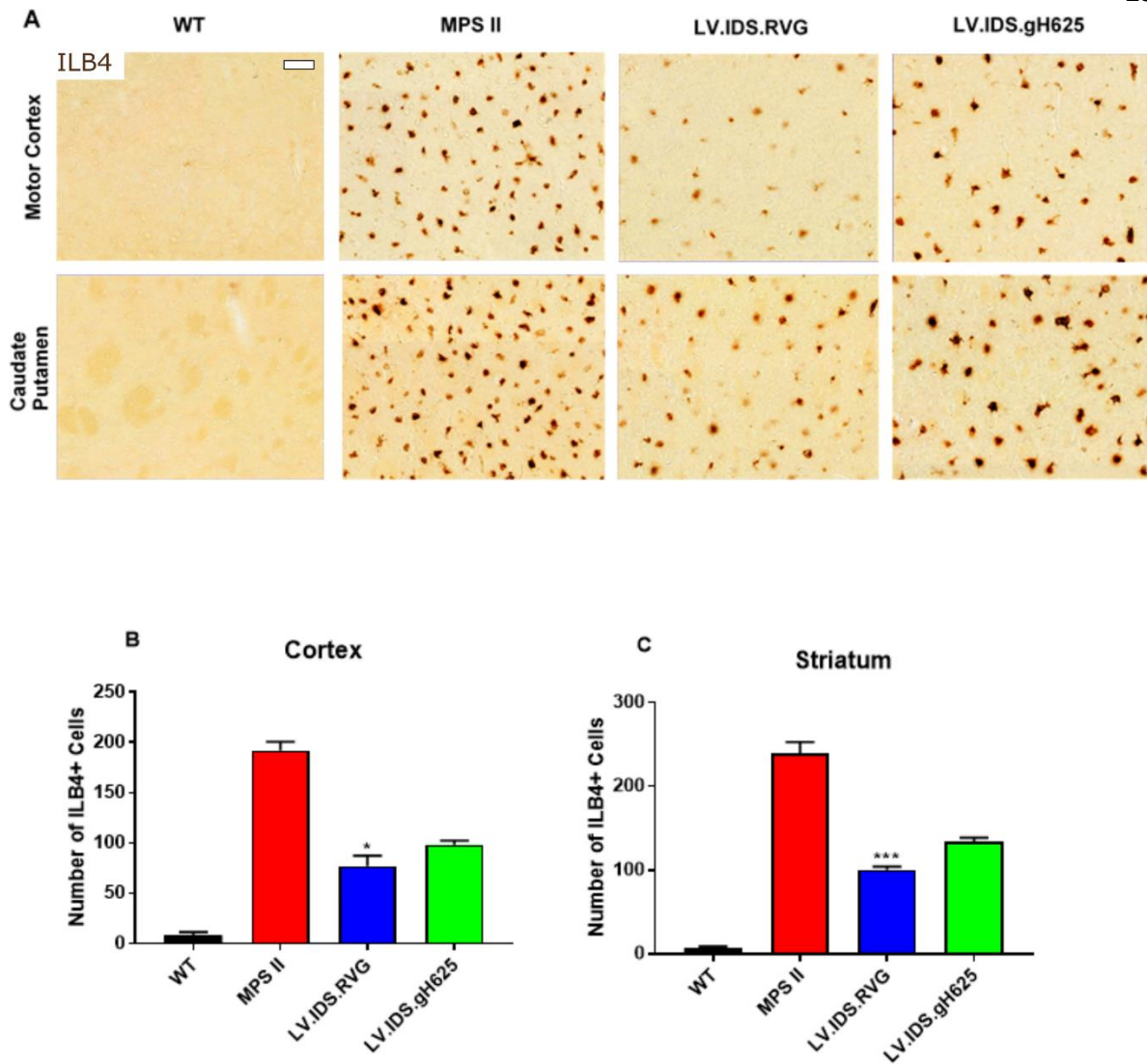


Figure 5. Significant reductions in number of activated brain microglial cells with LV.IDS.RVG HSCGT. (A) Representative images of 30µm brain sections of the motor cortex and striatum stained with ILB4 (brown) to detect activated microglia from control and treated mice. Representative images are shown following staining of 4-7 mice per group. (B) and (C) Cell counts of ILB4-positive cells from two sections per mouse in the cortex and striatum, 20x. Scale bar = 50µm. (Kruskal-Wallis test for non-parametric testing *=p<0.05). Data is displayed as mean ± SEM, * = p<0.05, *** = p<0.001 compared to MPSII.

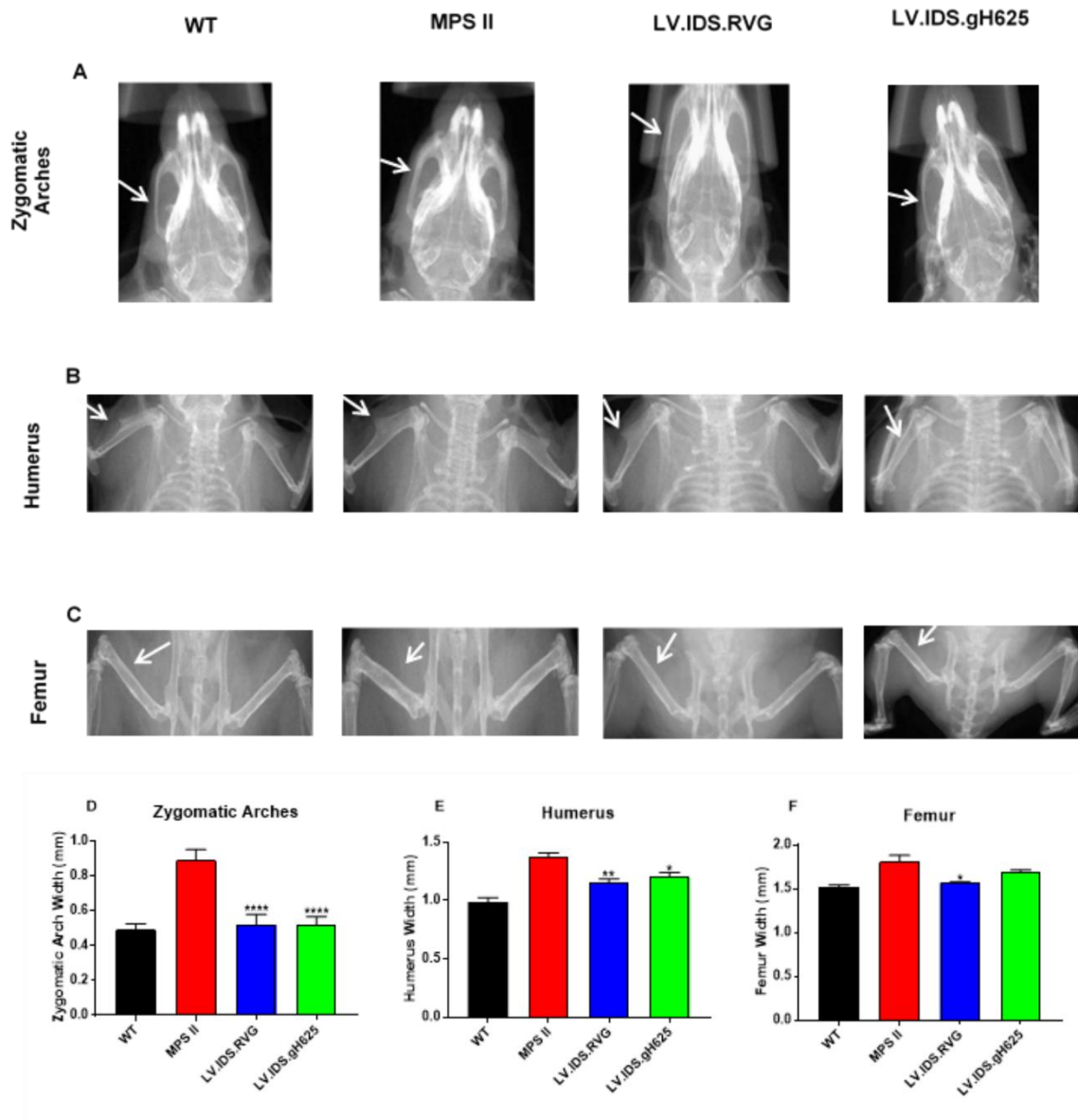


Figure 6. Skeletal defects are normalised by LV.IDS.RVG to WT levels and show reduction in bone width by LV.IDS.gH625 HSCGT. (A), (B) and (C) Representative X-ray images of control and treated MPS II mouse craniums, humerus and femurs. White arrows indicate where measurements are taken from. ImageJ software was used to analyse zygomatic arch widths (D), humerus widths (E) and femur widths (F). Data is displayed as mean \pm SEM, * = $p < 0.05$, ** = $p < 0.01$, **** = $p < 0.0001$ compared to MPSII via one-way ANOVA.